Uranium retention in a Callovo-Oxfordian clay rock formation: From laboratory-based models to in natura conditions

Gilles F Montavon, Solange Ribet, Y. Hassan Loni, F. Maia, C. Bailly, Karine David, Catherine Lerouge, B. Madé, J.C. Robinet, Bernd Grambow

Uranium retention in a Callovo-Oxfordian clay rock formation: From laboratory-based models to *in natura* conditions

G. Montavon[1]*, S. Ribet[1], Y. Hassan Loni[1], F. Maia[1], C. Bailly[1], K. David[1], C. Lerouge[2], B. Madé[3], J.C. Robinet[3] and B. Grambow[1]

(1) SUBATECH, IMTA/CNRS-IN2P3/Université de Nantes, 4, rue Alfred Kastler, F- 44304 Nantes

(2) BRGM, 3 avenue Claude Guillemin, F-45060 Orléans

(3) ANDRA, 1/7 rue Jean Monnet, Parc de la Croix-Blanche, F-92298 Châtenay-Malabry

*Corresponding author: montavon@subatech.in2p3.fr

Phone: +33 2 51 85 84 20

Keywords: U, COx, adsorption, lability, nuclear waste

Abstract

For the performance assessment of radioactive waste disposal, it is critical to predict the mobility of radionuclides in the geological barrier that hosts it. A key challenge consists of assessing the transferability of current knowledge on the retention properties deduced from model systems to *in natura* situations. The case of the redox-sensitive element uranium in the Callovo-Oxfordian clay formation (COx) is presented herein. Extensive experimental work was carried out with respect to parameters affecting uranium speciation (pH, P_{CO2}, [Ca] and

redox potential) with illite, COx clay fraction and raw COx claystone. The "bottom-up" approach implemented, with illite and montmorillonite as reactive phases, quantitatively explains the adsorption results of U(VI) and U(IV) on COx. While retention is high for U(IV) (Rd~10^4 L·kg^{-1}), it remains very low for U(VI) (Rd~4 L·kg^{-1}) due to the formation of soluble ternary Ca(Mg)-U(VI)-carbonate complexes. The applicability of the sorption model was then assessed by comparing predictive analyses with data characterizing the behavior of naturally-occurring U (<3 mg·kg^{-1}). The COx clay phase is the largest reservoir of naturally-occurring U (~65%) but only a small fraction appears to be adsorbed (~1 %). Under representative site conditions (especially with respect to reducing conditions), we have concluded that ternary U(VI) complexes control U speciation in solution while U(IV) surface species dominate U adsorption, with Rd values > 70 L.kg^{-1}.

1. INTRODUCTION

The disposal of radioactive waste in deep geological formations has been a topic of debate for many decades. The rationale lies in isolating the waste packages within specifically engineered facilities located deep underground (often 400 to 600 m) in geological formations in order to ensure that the time for fractions of the confined radionuclide inventories to potentially migrate to the human accessible environment remains much longer than their half life so as to protect future generations from radiological and chemotoxic risks. The main types of host rock formations used are sedimentary (e.g. clay rocks), crystalline (e.g. granite) or salt domes (Altmann, 2008).

Several countries are investigating claystone formations (e.g. Opalinus claystone (OPA) in Switzerland, Boda claystone (BODA) in Hungary, Boom clay (BC) in Belgium and Callovo-Oxfordian claystone (COx) in France). The COx formation is located in the eastern part of the

Paris Basin (depth: ~400-600 m, thickness: ~120-150 m) and is characterized by low permeability, mineralogical homogeneity and a low variation in other physicochemical properties over a large expanse (ANDRA, 2005).

Uranium and its decay series nuclides are a significant component of radioactive waste. Given a reducing environment measured in COx in the natural state (Eh ~ –190 mV), geochemical modeling exercises applied to radioactive waste disposal are able to predict U(IV) as the principal redox state in the formation when using a thermodynamic database, such as the Nuclear Energy Agency's Thermochemical Database (NEA-TDB) published in 2003 (Guillaumont et al., 2003). U(IV) species can be considered as immobile due to both their very high reactivity with claystone (sorption on clay mineral surfaces) and poor solubility in pore water. However, studies have identified soluble ternary complexes Ca-U(VI)-carbonate with strong formation constants (Bernhard et al., 1996; Dong and Brooks, 2006), thus shifting the U(VI)/(IV) stability field boundaries to more negative redox potentials; these complexes are expected to stabilize the U(VI) form under reducing conditions like those in COx claystone. Should the ternary aqueous complexes be stable and dominant, then uranium would become more soluble and mobile, even if U(IV) remains dominant in the solid phase. This outcome has recently been shown for OPA by means of a detailed modeling effort using one-dimensional diffusion models (Hennig et al., 2020).

For this reason, special care must be taken when dealing with uranium, since it is considered to be potentially the most mobile of the long-lived actinides in the performance assessment.

To date, just one work has been devoted to U(VI) retention on COx (Hartmann et al., 2008). These authors showed the importance of ternary complexes in describing the data, but their model was unable to satisfactorily reproduce the experimental results. Furthermore, all studies on claystones (COx, BODA or OPA) focus on the retention of U(VI) (Amayri et al., 2016;

Bradbury and Baeyens, 2011; Hartmann et al., 2008; Joseph et al., 2011; Kautenburger et al., 2019; Marques Fernandes et al., 2015), although to the best of our knowledge no experimental data on U(IV) actually exist. Along the same lines, only the U(VI) retention model has been taken into account to simulate the diffusion of U in the OPA formation (Hennig et al., 2020). Given the highly reducing environment of deep formation, a major role played by the tetravalent state of U on uranium retention cannot be excluded.

Given the limited number of published articles, lack of data (notably with respect to U(IV)) and importance of the topic, the objective of this work is to promote a better understanding of uranium retention in the Callovo-Oxfordian formation. The term retention, as used herein, means the adsorption of U on the clay fraction governed by kinetically fast and reversible adsorption processes (ion-exchange, surface complexation) (OECD Nuclear Energy Agency, 2002). Throughout this paper, the term “labile fraction” will be used in order to characterize the adsorbed U fraction in “equilibrium” with the water-soluble part over a short time scale, whereby the formation can be described by local equilibrium approaches. The significance of the clay fraction for metal adsorption by COx has already been shown for Cs (Chen et al., 2014b), Ni (Chen et al., 2014a; Grangeon et al., 2015; Montavon et al., 2020) and Eu (Loni et al., 2021). Such is also the case for Opalinus Clay, whose mineralogy is quite close (Bradbury and Baeyens, 2011; Marques Fernandes et al., 2015).

In this exercise, extensive experimental work has been carried out under well-controlled conditions with illite, the COx clay fraction and raw COx by studying the parameters affecting uranium speciation (pH, P_{CO2}, presence of divalent cations (Ca, Mg), redox potential). The available 2-Site Protolysis, Non-Electrostatic Surface Complexation and Cation Exchange model (2 SPNE SC/CE), proposed by Bradbury and Baeyens (1997) and developed for OPA, has been used as a basis for describing the data in relying on the simplifications proposed in the literature for COx (Chen et al., 2014a; Grangeon et al., 2015;

Tournassat et al., 2009). Special attention has been paid to the U(VI)/illite/carbonate system in order to better assess the role of ternary surface complexes, ≡S-U(VI)-carbonates, in light of the absence of specific data for illite in the published models (Bradbury and Baeyens, 2017). These data then make it possible to develop an operational model that allows predicting the adsorption properties of uranium under *in natura* COx conditions by pursuing the "bottom-up" approach with very good knowledge of the COx environment (Gaucher et al., 2009; Lerouge et al., 2011).

Inspired by previous work focusing on uranium-contaminated areas (Curtis et al., 2004; Kohler et al., 2004; Payne et al., 2001), these predictions were subsequently compared with results describing the behavior of uranium naturally present in the formation at trace concentrations. In addition to the analysis of U distribution in the various COx reservoirs, emphasis has been placed on the labile part of this element, i.e. a fraction difficult to characterize under conditions of trace concentrations, when spectroscopic tools are not applicable (McKinley and Alexander, 1993). This fraction is needed in order to compare the data with results obtained in the laboratory; it has been estimated by means of sequential extraction (Claret et al., 2010), isotope exchange (Ahmed, 2014) and by following a desorption method successfully tested on the Ni/COx system (Montavon et al., 2020).

In sum, the challenge of this work lies in linking the model system to the natural system and drawing a conclusion on the degree to which uranium remains mobile in the COx formation; the steps involved must identify which physicochemical parameters control uranium mobility from a mechanistic point of view.

2. EXPERIMENTAL DETAILS

2.1 Materials

119 *2.1.1 Chemicals*

120 All solutions were prepared with ultra-pure deionized water (18.2 MΩ.cm) and commercially
121 available chemical products of analytical or ultra-trace metal grade. For HR-ICP-MS
122 measurements, nitric acid was purified using a sub-boiling distillation system (Savillex DST-
123 1000). U(VI) stock solution was prepared from ICP standard solution (1,000 µg/mL in 4%
124 HNO_3 or 10,000 µg/mL in 0.4% HNO_3) (SCP Science, France). The solution of ^{233}U was
125 provided in 2N HNO_3 at an activity of 231 Bq (0.65 µg) of ^{233}U per gram of solution
126 (Amersham). ^{232}U (841 $kBq.g^{-1}$ in 2N HNO_3 - CERCA) was also used as a tracer for some of
127 the experiments performed under reducing conditions.

128 *2.1.2 COx samples*

129 All COx samples used in the present study are core samples from boreholes within the studied
130 area (Meuse/Haute-Marne, France). The claystone consists (in percentage by weight) of a
131 major clay fraction (40-60%), associated with both quartz (25-37%) and carbonate (12-32%)
132 fractions. The clay minerals are mainly illite (ILL) (14-29%) and ordered illite-smectite mixed
133 layers (IS) (18-33%), with minor kaolinite and chlorite contents (Lerouge et al., 2011).

134 This work has benefited from a collection of some 50 samples extracted from various units
135 and characterized in terms of composition and trace elements (Lerouge et al., 2006). Other
136 samples were selected for the experimental work with two objectives, namely: (i) evaluation
137 of the U distribution in the COx in order to identify the U-carrier phases by correlating the
138 measured concentrations with sample characteristics; and (ii) execution of the laboratory
139 experimental campaign. Detailed information on these samples is given in Table A-1. Except
140 for sample EST21400, which is rich in calcite, the samples were all extracted in a unit with
141 maximum clay content (40%-53%). After drilling, they were conditioned in airtight aluminum
142 foil filled with nitrogen, transported to the laboratory and then stored until their opening in a
143 N_2/CO_2 (1%) glove box.

144 The separation and purification of the COx clay fraction (COX-cf) (from EST51779) was
145 performed by elutriation and chemical purification, as provided by the BRGM Institute
146 (Claret et al., 2004). The sample labeled EST25687(ox) corresponds to a portion of the
147 previously preserved EST25687 sample analyzed in 2006 and not preserved since then.
148 Analyses conducted on both oxidized and non-oxidized samples allow assessing the potential
149 presence of reduced forms of uranium. Furthermore, sample EST26536 was selected in the
150 maximum clay zone for its phosphate nodules.

151 Water samples from three drillings, cored with inert gases (N_2 or Ar), were analyzed in order
152 to define the representative U concentration values in the pore water of the Callovo-Oxfordian
153 (PAC1002, POX1201, EPT1201) (Vinsot et al., 2013). Data were also collected from
154 GIS1002 (Grangeon et al., 2015); although initially drilled under unpreserved conditions, a
155 state of return to *in natura* equilibrium can now be observed. The effect of an oxidative
156 disturbance on the U pore water concentration has been evaluated from borehole KEY1001
157 (Grangeon et al., 2015).

158
159 *2.1.3 Aqueous media*

160 Synthetic pore water (SPW1) representative of the COx formation, and in equilibrium with
161 calcite, was prepared under controlled anoxic Ar/CO_2 conditions ($P_{CO2} = 10^{-2}$ atm or 1%) for
162 the sorption experiments with illite, COx-cf and COx and for the purpose of evaluating the
163 labile part of naturally-occurring U (Table A-2).

164 These experiments were also carried out in weakly complexing media ($NaNO_3$ or NaCl) with
165 an ionic strength (0.1 M) close to that encountered *in natura*. Various atmospheres were
166 selected (Ar, air/CO_2 at atmospheric pressure ($10^{-3.5}$ atm), 1% CO_2 (10^{-2} atm) and 5% CO_2
167 ($10^{-1.3}$ atm)) in order to evaluate the impact of carbonates on the retention of uranium onto

168 illite. Equilibrium with P_{CO2} was verified qualitatively, after at least one day of equilibration
169 while the pH was stable, and quantitatively via an alkalinity measurement.

170 The effect of redox potential was also evaluated under inert atmosphere (Ar) and in the
171 presence of carbonates (3,500 ppm or 9,500 ppm CO_2) in synthetic groundwater SPW2 (Table
172 A-2). In order to promote the conditions to have U(IV), a reducing agent (Na_2S) was added to
173 the system.

174

175 **2.2 Batch-type experiments**

176 A summary of the experimental campaign is given in Table 1 and detailed experimental
177 conditions are provided in the appendices (Tables A-3 and A-4).

178 All experiments were performed at room temperature (T = 22° ± 3°C) in polypropylene
179 copolymer (PPCO) tubes either inside or outside the glove box, depending on the desired
180 atmosphere. Moreover, they were conducted under conditions whereby uranium did not
181 precipitate; these conditions were first deduced from simulations (see the "Modeling" section
182 below, 2.4) before being verified for an absence of precipitation by filtration using 0.45-µm
183 PolyTetraFluoroEthylene (PTFE) filters.

184 The data on adsorption experiments were acquired using the classic batch-type technique
185 (Montavon et al., 2006). The solid phase was equilibrated with the liquid phase before adding
186 U to the system. Note that for the experiments with Na_2S, the reducing agent was added both
187 to the U stock solution and to the suspension. In the end, the Eh value measured under
188 equilibrium conditions was taken into account for the data analysis. Preliminary sorption
189 experiments showed that a contact time of 3 days was sufficient to reach sorption equilibrium
190 conditions (data not shown). The solid and liquid phases were separated by means of filtration
191 using 0.2-µm PTFE or Surfactant-free Cellulose Acetate (SFCA) filters. Except for the

192 experiments carried out under inert conditions (Ar), no sorption at the surface of tubes or on
193 filters could be detected (< 5%). When such was not the case (experiments under Ar
194 atmosphere), a correction was introduced based on a "blank" analysis (i.e. under the same
195 conditions but in the absence of the sorbent phase). The pH values of the solutions and
196 alkalinity were measured at the end of the experiments. This step also applied to experiments
197 carried out under Ar atmosphere, wherein carbonate traces can affect the speciation of U
198 (Tournassat et al., 2018). The distribution coefficient between solid and liquid phases, Rd (in
199 $L \cdot kg^{-1}$), was defined as follows:

200 $$R_d = \frac{[U]_0 - [U]_{aq}}{[U]_{aq}} \frac{V}{m} \quad (1)$$

201 where $[U]_0$, $[U]_{aq}$, m and V denote the U concentration introduced in the system ($mol \cdot L^{-1}$), the
202 U concentration measured in solution at equilibrium ($mol \cdot L^{-1}$), the solid mass (kg) and the
203 solution volume (L), respectively.

204 This same batch-type method was followed for experiments carried out with naturally-
205 occurring U in order to quantify the labile fraction, in considering an isotopic exchange
206 approach (Ahmed, 2014) and a desorption study (Montavon et al., 2020). The equilibration
207 criteria will be presented in the "Results" section. For the desorption experiments, if U in the
208 aqueous phase is controlled by an adsorption equilibrium and given the assumption that the
209 Rd model is applicable, the following relation is obtained for correlating the U concentration
210 in the aqueous solution (in $\mu g \cdot L^{-1}$) with the solid-to-liquid ratio m/V (in $g \cdot L^{-1}$):

211 $$[U]_{aq} = \frac{n.\frac{m}{V} + [U]_i}{\left(1 + Rd.\frac{m}{V}\right)} \quad (2)$$

212 where $[U]_i$ represents the potential contamination of U initially present in SPW (in $\mu g \cdot L^{-1}$),
213 and *n* the quantity of mobilizable element ($\mu g \cdot g^{-1}$), i.e. the labile quantity associated with COx

plus the quantity initially present in pore water and present on the raw solid (in $\mu g \cdot g^{-1}$). The Rd unit of measurement used in this expression is $L \cdot g^{-1}$.

2.3 Analytical procedures

2.3.1 Aqueous solutions

Uranium was measured in aqueous solutions by ICP-MS (Thermo Xseries 2, Thermo Scientific) when concentrations were above 2 µg/L and HR-ICP-MS for U concentrations at ultra-trace level (Element XR, Thermo Scientific). Quantitative analyses of uranium were performed by external calibration with a set of gravimetric uranium standard solutions prepared using an internal standard solution of thallium in 2% (v/v) HNO_3 for correction of matrix effects and instrumental drift.

^{232}U analyses were performed by liquid scintillation counting with a Packard TriCarb 3170 TR using an Ultima Gold LLT® (Perkin Elmer) scintillation cocktail. ^{232}U / ^{228}Th separation was carried out prior to analysis using the anionic exchanger Dowex 50WX8-200 with 8M HCl as elution medium for thorium while uranium remains on the resin. Then ^{232}U was ultimately recovered with water.

Alkalinity was determined by colorimetric analysis using Bromocresol Green-Methyl Red pH- indicator powder pillow and a Digital Titrator (Hach method 8203) with digital titrator cartridges containing 0.16 N (or 0.02 N for a low concentration of carbonates in the system) of H_2SO_4.

pH values were measured by a pH-meter combined with a pH electrode and thermometer detector (pHC2085, Hach Lange) of hydrogen ion activity. The pH electrode was composed of glass combined with a red rod reference electrode of silver/silver chloride. The pH-meter was automatically calibrated by PHM220 Lab pHmeter (Radiometer Analytical) at the

beginning of each experiment using two standard IUPAC buffer solutions of pH 4.005 and 7.000 (Radiometer Analytical).

The redox potential was measured by a pH-meter combined with a redox electrode (MC3051-PT-9, Radiometer Analytical). This electrode had an Ag/AgCl reference system with a refillable electrolyte (3 M KCl saturated with AgCl), porous pin junction and platinum ring sensor. The electrode was calibrated with a redox standard solution; its values were given with respect to the normal hydrogen electrode (NHE).

2.3.2 COx phases

The sequential extraction protocol adapted from Claret et al. (2010) was first used to assess the U distribution in the COx clay. The extraction steps comprised the following:

Fraction 1 (F1 - water soluble fraction): The extraction was performed in the glove box (Ar atmosphere), where 20 mL of deionized water were added to 4 g of solid sample and shaken for 24 h. The resulting solution was then filtered using 0.22-µm Surfactant-Free Cellulose Acetate filters after centrifugation at 20,000 rpm for 10 minutes.

Fraction 2 (F2 – part of the adsorbed fraction): In this step, as well as for steps 3 through 5, the extractions took place outside the glove box. 20 mL of hexamine trichloride (4.458 $g \cdot L^{-1}$) were mixed with the residue from the previous step and shaken for 30 minutes. After centrifugation and filtration, the solid obtained was used for step 3.

Fraction 3 (F3 – part of the adsorbed fraction and U present in carbonate phases): 20 mL of an acetate/acetic acid buffer at pH 5 were added to the residue from the previous step and then shaken for 12 h. After centrifugation and filtration, the solid fraction was used for the next step.

Fraction 4 (F4 - organic matter fraction): 20 mL of H_2O_2 at pH 2 (adjusted using HNO_3) were added to the residue of the previous extraction and heated at 50°C for 3 h. After centrifugation and filtration, the solid fraction was used for the final step.

Fraction 5 (F5 - residual fraction): In this last step, the sample was digested by a sequence of: dissolution in a mixture of HNO_3 (2 mL), HF (10 mL) and $HClO_4$ (5 drops) at 120°C for one week followed by the evaporation of HF, and then the addition of HCl 6N (10 mL) at 100°C for one week.

The same digestion procedure was also carried out on COx samples of interest for the determination of total concentration of U naturally present. It should be noted that a digestion procedure was also conduct to dissolve the organic matter separated by handpicking from the EST26536 sample under the binocular lens; to accomplish this, 20 mL of an H_2O_2 solution at pH 2 (adjusted using HNO_3) were used at 50°C for 3 hours. Also note the absence of any visible residue after extraction indicating the purity of the separated organic matter.

U solid analyses were performed by laser ablation HR-ICP-MS. Details of the instrumental facility, optimization strategy of laser and HR-ICP-MS instrument, data acquisition and off-line processing are reported elsewhere (Loni et al., 2021; Montavon et al., 2020). The certified value of U concentration at 37.38 $mg.kg^{-1}$ of the NIST 612 standard reference material was used for uranium quantification in COx mineral phases by external calibration and internal standardization (Loni et al., 2021; Montavon et al., 2020). The total analysis time for laser ablation sample and gas blank measurements is reported in Table S1. The sample had previously been mounted on a glass blade with an epoxy-type glue, and its surface polished by silicon carbide grinding paper (Struers) (grading size: from 80 to 4,000 Grit).

2.4 Modeling considerations

All calculations were carried out with the PhreeqC code (version 3.2.1) (Parkhurst and Appelo, 2013). The Davies equation (Davies, 1962) was used for the ionic strength correction of solutes with the corresponding THERMOCHIMIE v10a (2018) database (Grivé et al., 2015), www.thermochimie.org) . The stability constants of aqueous uranium species were extracted from the NEA Thermodynamic Database (Grenthe et al., 2020), except for $CaUO_2(CO_3)_3^{2-}$ and $Ca_2UO_2(CO_3)_3$ species, which were drawn from (Maia et al., 2021). . All relevant data can be found in the supplementary data section of this article (Table S2).

For the adsorption model, it was not sought to build a new type of model but rather to use existing models and test/adapt them to the COx conditions. We chose the 2SPNE SC/CE model (Bradbury and Baeyens, 1997) since it is the most complete among those available in the literature and had already been satisfactorily tested for both Ni/COx (Chen et al., 2014a; Grangeon et al., 2015; Montavon et al., 2020) and Eu/COx (Loni et al., 2021) systems. According to the 2SPNE SC/CE model, the surface complexation phenomenon is controlled by both weak (i.e. high quantity, limited affinity) and strong (low quantity, high affinity) sites. Previously published simplifications and assumptions (Chen et al., 2014a; Grangeon et al., 2015; Montavon et al., 2020; Tournassat et al., 2009) are considered herein, namely: (i) 2:1 clay minerals control the retention, and the potential contributions of chlorite and kaolinite are not taken into account in the overall sorption of uranium; (ii) the I/S interstratified layers are assumed here as two phases, where each phase corresponds to 50% wt. of illite and smectite, respectively; and (iii) montmorillonite is used as a proxy for smectite phases since it is an example of a well-studied smectite.

For the quantitative description of these adsorption experiments, the mineralogical compositions listed in Table A1 have been taken into account.

The adsorption parameters for both illite and montmorillonite are summarized in Table A5. Values for the U(VI) surface complexation reactions were taken from (Baeyens and Bradbury, 2017) for montmorillonite and from (Bradbury and Baeyens, 2017) for illite. Values for the U(IV) surface complexation reactions were calculated from the Linear Free Energy Relationship equations (Baeyens and Bradbury, 2017; Bradbury and Baeyens, 2017), as established from sorption data with Th(IV).

For the various modeling predictions, the average clay concentrations encountered in the formation (see previous section) have been used. As regards model sensitivity, unless otherwise stated, calculations were performed with the lower and upper clay content limits.

3. RESULTS

Based on literature data (Chen et al., 2014a; Grangeon et al., 2015; Montavon et al., 2020; Tournassat et al., 2009), it has been assumed that the COx clay fraction controls uranium adsorption. The adsorption mechanism, including both surface complexation and cation exchange, leads to the formation of so-called "labile" chemical forms, i.e. in rapid equilibrium with the fraction in solution. Other retention mechanisms such as incorporation or co-precipitation, which generally lead to so-called "inert" forms, were therefore neglected in our approach. The experimental and simulation approaches were oriented along these lines. The relevance of these assumptions, in particular when linking the model system to the natural system, will be discussed in Section 4.

3.1. Which model for describing U retention on COx?

3.1.1. Conditions where U(VI) species dominate

The experimental data obtained for illite under various experimental conditions are given in Figure 1. Maximum sorption was reached at a pH range between about 6.5 and 7.5. Under

conditions with a low carbonate level and simple background electrolyte, a retention value of $(4 \pm 0.3)\ 10^5$ L·kg^{-1} was calculated. With an increasing carbonate level (i.e. atmospheric CO_2 and 1% CO_2), a decrease in the Rd value was observed (Rd ~ $(3 \pm 0.5)\ 10^4$ L·kg^{-1} and ~$(2 \pm 0.4)\ 10^3$ L·kg^{-1}, respectively). In SPW containing divalent cations and a 1% CO_2 atmosphere, this decrease was even greater, with Rd values of approx. 45 ±9 L·kg^{-1}.

This trend has previously been observed for the retention of U(VI) on smectite in the presence of CO_2 (Marques Fernandes et al., 2012). If the formation of carbonate complexes (and in particular ternary complexes with divalent cations) lies at the origin of the retention decrease, then the data cannot be modeled when ignoring the sorption of uranyl-carbonate complexes. Similarly to the study by (Marques Fernandes et al., 2012) the formation of two surface complexes for illite are considered (Table A5):

$$\equiv sOH + UO_2^{2+} + CO_3^{2-} = \equiv sOUO_2CO_3^{-} + H^+ \qquad \text{Log } K_1 \qquad (3)$$

$$\equiv sOH + UO_2^{2+} + 2\ CO_3^{2-} = \equiv sOUO_2(CO_3)_2^{3-} + H^+ \qquad \text{Log } K_2 \qquad (4)$$

These constants have been (manually) adjusted to obtain a satisfactory level of agreement between the model and the experiment.

The model was then applied predictively to the COx clay fraction, under various experimental conditions, as well as to the COx clay rock in the presence of synthetic water (Fig. 2). For the clay fraction, in a simple background electrolyte, Rd values of $(8.0 \pm 0.8)\ 10^3$ L·kg^{-1} and $(2.0 \pm 0.2)\ 10^3$ L·kg^{-1} were obtained in close to atmospheric CO_2 pressure and 1% CO_2, respectively. In the presence of SPW, Rd decreased to about 50 ± 25 L·kg^{-1}. For the COx clay rock experiment, the retention coefficient decreased to low values, i.e. approx. 3.6 ± 1.5 L·kg^{-1}.

354 In sum, the retention coefficient varies in the following order: illite ~ COx-cf > COx, which
355 qualitatively shows that the clay fraction of COx is, in terms of reactivity, close to illite. These
356 data are on the whole well reproduced by the model, including the two new surface
357 complexation reactions (lines in Fig. 2).

358 The model was ultimately tested with data published for U/clayey rock systems (Fig. A1,
359 Table S3); the output provides a satisfactory explanation of the experimental data, within the
360 uncertainty, for BODA and OPA, as do the modeling approaches proposed in the referenced
361 papers. Despite producing better results, the experiment / calculation agreement was still not
362 perfect for the data held by Hartmann et al. (2008) (Fig. A1c). Note that in their work, the
363 sorption of uranyl on COx claystone was studied at 0.1 M $NaClO_4$ in atmospheric CO_2
364 pressure as a function of pH and with an assumption of calcite equilibrium.

365 *3.1.2 Impact of reducing conditions*

366 Given the highly reducing environment for the deep formation of COx, a significant role
367 played by the tetravalent state of U on uranium retention cannot be excluded. This hypothesis
368 has therefore been tested from batch-type experiments with the EST05640 sample. The
369 corresponding experimental conditions are shown in the appendices (Table A4).

370 The experimental data are given in Figure 3, along with the model predictions. As expected,
371 retention was strong with Rd values on the order of 10^4 $L \cdot kg^{-1}$. Although the experimental
372 data were rather scattered, the agreement between experiment and calculation appears to be
373 relatively good, with no parameter adjustment being required. Modeling results indicate that
374 U(IV) dominates the surface speciation for all studied conditions (> 99.6%). It is also the
375 major redox state in solution for the conditions presented in Figures 3a and 3b (99% and 90%,
376 respectively) but not in the presence of 9,500 ppm CO_2, where it corresponds to only 10%
377 (Fig. 3c).

3.2. Distribution of naturally-occurring U in COx

In the COx formation, uranium contents are low, i.e. between 0.5 and 2.4 $mg \cdot kg^{-1}$ (Fig. 4a). Among the various samples whose U amount has been analyzed, a distinct correlation exists with the organic matter: the higher the organic matter (OM) concentration, the greater the amount of U (Fig. 4a). For the samples used in laboratory studies, the upper concentration limit is reached, i.e. between 2 and 3 $mg \cdot kg^{-1}$.

Among the various phases, uranium is expected to be incorporated in minor phases, e.g. phosphates (Regenspurg et al., 2010). Calcite might be another possible reservoir due to its high reactivity and ability to trap metals (Zhao and Zheng, 2014). These minerals were therefore singled out in the present study, which also considered organic matter (in relation to the correlation presented above) as well as the clay fraction, given its predominant role in the metal adsorption process. Analysis details can be found in Table S1.

The analyses of individual mineral phases carried out on sample EST51769 yielded U concentration values of 2.7 ± 0.8, 1.0 ± 0.3 and 0.013 ± 0.004 $mg \cdot kg^{-1}$ for clay, calcite and pyrite fractions, respectively. Similar results were observed for biocalcite and diagenetic calcite on the EST05738 and EST26536 samples; the values were 0.4 ± 0.2 and 0.5 ± 0.3 mg kg^{-1}, respectively. Four calcium phosphate analyses (EST26536) were performed in line mode and the average uranium content equaled 32 ± 4 $mg \cdot kg^{-1}$. Lastly, the uranium concentration measured in organic matter led to a U content of 69.2 $\mu g \cdot kg^{-1}$.

Considering the average composition of COx in the clay-rich zone and the U concentration measured for EST51769 (whose main values were obtained), the distribution diagram shown in Figure 4c is derived (due to the low levels measured, U concentrations in pyrite and organic matter are not reported).

The U concentration of the bulk rock (called total (ind.) in Fig. 4c), as recalculated from the U concentrations measured in the various phases and their proportion in the COx, corresponds (within the range of uncertainties) to the U concentration measured directly in the bulk rock (called total in Fig. 4c). This finding indicates that the major carrier phases have been identified. While the highest U concentrations were found in phosphate minerals, as expected, the clay fraction actually corresponds to the greatest reservoir with ~65% of the uranium present. On the other hand, Figure 4a serves as an "optical illusion" since the organic matter, due to its low quantity in the COx and low U concentration measured in this phase, is clearly not a U-bearing phase. The origin of this visual correlation remains unclear and has not been further investigated herein, given the objectives of this work.

The uranium distribution was then indirectly evaluated by means of sequential extraction; results are shown in Figure 4b. Distributions are similar for all clay-rich samples (~3 $mg \cdot kg^{-1}$ in U). The U in fractions F1 (water soluble fraction), F2 (part of the adsorbed fraction) and F4 (organic matter fraction) accounts for less than 5% of total U. This result is consistent with previous data; U in the organic fraction (F4) can be neglected. Therefore, U is mainly distributed between fractions F3 (part of the adsorbed fraction and U present in carbonate phases) and F5 (residual fraction), with a relatively constant distribution of ~12%:86% F3:F5. Moreover, no significant effect was observed relative to the state of conservation of the COx.

At this stage, it is interesting to compare these sequential extraction results with analyses conducted directly on solids. The uranium fractions present in carbonate phases and on clays (assuming that U is adsorbed) should mostly be found in F3 (the adsorbed part of U found in F2 being considered negligible). If we consider that the uranium in phosphates is trapped in the matrix, a proportion between fractions F3 and F5 on the order of 90%:10% is thus obtained from the direct solid analyses presented in Fig. 4c. While this analysis is consistent with sequential extraction results from a qualitative point of view, such is not the case from a

quantitative point of view; in fact, the inverse trend is observed, i.e. ~12%:86% F3:F5. Since the carbonate phases are completely dissolved after step 3, a sizable fraction of the U directly detected in the clay phase is present in a "non-labile" form, i.e. not desorbed with the pH decrease and thus recovered in F5. The U content measured in the F3 fraction therefore stems mainly from the dissolution of carbonate phases.

This result is consistent with the fact that the F3 fraction increases with the amount of carbonate phases, that is ~35% and ~12 % for EST21400 (~81% of carbonate phases) and EST26536, EST25687 and EST26480 (~25% of carbonate phases), respectively. From a quantitative point of view, assuming that the uranium in the clay fraction is completely found in F5, in knowing the carbonates phases content of the COx samples (Table 1), a U content of ~1.3 $mg \cdot kg^{-1}$ and ~0.9 $mg \cdot kg^{-1}$ in the carbonate phases can be recalculated from the sequential extraction results (F3) for samples rich in clay and carbonate phases, respectively. The order of magnitude is consistent with that found from direct analysis of calcite (the majority phase of carbonate phases), i.e. ~0.4-1 $mg \cdot kg^{-1}$.

In conclusion, if uranium is mainly present in the COx clay fraction, it is not retained (for a large part) in a form expected by our model, namely retained by a surface complexation mechanism.

3.3. Retention coefficient and labile fraction of naturally-occurring U under both oxidizing and reducing conditions

Experiments were conducted with COx powder in the presence of SPW1 under Ar/CO_2 atmosphere.

Results of the isotope exchange method are given in Figure 5a. A fraction of the naturally-occurring U was rapidly resupplied from the clay rock samples in solution, with steady state

451 achieved after less than 1 day of contact. Regarding the samples doped with ^{233}U, about 3
452 days were required to reach steady state. We consider that this contact time is insufficient to
453 allow for the exchange of U-233 with U-238 incorporated into the mineral matrix; since this
454 process is controlled by solid diffusion, the kinetics are expected to be very slow. An analysis
455 of the data yields an Rd value of 7.6 ± 2.3 $L \cdot kg^{-1}$ and an amount of labile U present in the
456 COx of 26 ± 7 $\mu g \cdot kg^{-1}$.

457 For the desorption method, like for the isotope exchange method, contact time is a critical
458 parameter to be assigned. While the time to reach steady state is quick at m/V=50 $g \cdot L^{-1}$, it still
459 might vary with respect to the solid-to-liquid ratio. Two other kinetic experiments were
460 therefore performed for lower solid-to-liquid ratios (i.e. 0.5 and 1 $g \cdot L^{-1}$). The equilibration
461 time was longer (i.e. 4 days instead of 1 day) (Fig. 6b), and a contact time of 7 days was thus
462 set for all experiments.

463 The desorption results obtained as a function of the solid-to-liquid ratio are provided in Figure
464 5c. Like with the sequential extraction results, no difference has been found between the
465 preserved (black symbols) and unpreserved (white symbols) COx samples. The experimental
466 data can be well explained in considering our simple model (Eq. 2) with Rd and *n* values at
467 8.0 ± 4.6 $L \cdot kg^{-1}$ and 30 ± 12 $\mu g \cdot kg^{-1}$, respectively (solid lines in Fig. 5c). Note that the
468 uranium content present in SPW1 as well as the amount of U in COx originating from pore
469 water are both negligible quantities. The good agreement of results between the two
470 equilibrium-based methods have given us confidence in the results. It should also be noted
471 that although the isotope exchange method does make it possible to return to a value for the
472 distribution of uranium (VI) between solid and liquid phases (as translated by an Rd value),
473 the desorption method, owing to the curve shape, exposes this as an adsorption phenomenon.
474 If in fact it was controlled by a solubility mechanism, then the U concentration would not
475 evolve with the mass-to-volume ratio (under saturated conditions).

476 A final experiment was carried out in the laboratory to assess the relevance of redox potential.
477 A suspension at 50 $g \cdot L^{-1}$ of COx (leading to a measured U concentration of 0.99 $\mu g \cdot L^{-1}$ for
478 Eh~0 mV / NHE) remained in the glove box (Ar/CO_2) for nearly 3 years. The measured
479 potential dropped back to the characteristic value of the site (i.e. Eh~-200 mV) and the U
480 concentration decreased by a factor of nearly 10 (gray symbols in Fig. 5c). By considering the
481 labile fraction of U as a fixed parameter, this implies that U speciation at the surface has
482 changed, which results in an increase in the Rd value from 8.0 ± 4.6 to 500 ± 200 $L \cdot kg^{-1}$.

483

484 **4. DISCUSSION**

485 An operational model, based on both a bottom-up approach and the 2SPNE SC/CE model, has
486 made it possible to quantitatively describe uranium sorption onto illite, the clay fraction of
487 COx and COx clay rock for a wide variety of conditions sensitive to U specification (pH, Eh,
488 pCO_2, concentration of divalent cations (Ca^{2+}, Mg^{2+})). Compared to the available adsorption
489 database, two parameters had to be fitted, namely the constants describing formation of the
490 ternary surface complexes with illite and U(VI) (Eqs. (3) and (4)). Note that the existence of
491 such carbonato surface complexes has recently been questioned in describing the U(VI) /
492 montmorillonite system (Tournassat et al., 2018). The formation of secondary sites
493 $\equiv sOH_2CO_3^-$ and $\equiv sOH_2HCO_3$ able to assist modifying metal retention (Rieder, 2019) can also
494 be envisaged. Given the objective of the present work, this aspect has not been further
495 explored.

496 Thanks to the operational model, it was possible to analyze the results of equilibrium-based
497 methodologies describing the behavior of the naturally-occurring U labile fraction for a
498 COx/SPW1 system representative of the natural environment. In terms of “oxidizing”

conditions, this labile fraction is characterized by an Rd value of ~8 $L.kg^{-1}$. According to the model, this finding reflects the presence of U(VI) adsorbed onto the clay surface. Such a result validates the hypothesis of the clay fraction controlling the U adsorption process. The labile fraction however remains low compared to that measured directly by LA-HR-ICP-MS in the clay phases (~1% of total U content). This result confirms our previous hypothesis that a significant fraction of uranium found in the COx clay fraction is in fact incorporated into the matrix in an "inert" form, as found in the residual fraction of the sequential extraction experiments.

In conclusion, we can consider a labile fraction of naturally-occurring U in the formation on the order of 30 ± 12 $\mu g.kg^{-1}$, to be associated with the clay fraction in an adsorbed form.

At this stage, the purpose of this work is to correlate the results obtained with the information available at the geological formation level, i.e. the concentrations of U in the pore water.

Since no uranium phase has been observed and the labile fraction of naturally-occurring U was found to be adsorbed onto the clay fraction (in the form of U(VI)), we can forward the assumption that *in natura* pore water concentration is also controlled by an adsorption phenomenon. Based on this assumption, the range of *in natura* concentrations in pore water can be predicted from Eq. (2), in knowing: the labile fraction of U, the Rd value (as characterized by the presence of U(VI)), and the high solid-to-liquid ratio characterizing the site (~8% wt. of water, i.e. ~11,500 $g.L^{-1}$). A range of aqueous U concentrations between 1.4 and 12 $\mu g.L^{-1}$ can thus be calculated (solid lines, Fig. 5c).

It is now important to compare this concentration range, deduced from the laboratory experiments, with that measured directly in the pore water collected at the various boreholes (see Section 2.1.2). A value of 0.13 $\mu g.L^{-1}$ has been selected by ANDRA; this value lies close to that measured in this study for the GIS1002 borehole, i.e. 0.25 ± 0.02 $\mu g.L^{-1}$. It also lies

close to the value measured under the undisturbed conditions of the DIR experiment (0.24 $\mu g.L^{-1}$) (Fralova, 2020). The results are therefore very consistent, and a concentration range of 0.13-0.25 $\mu g.L^{-1}$ can be given as representative values of the COx formation.

This range appears to be more than 10 times lower than the values deduced from Eq. (2); this information immediately suggests that laboratory experiments are not representative of the natural system.

The uncontrolled parameters in the laboratory are the COx state and redox potential. Three articles focus on the effect of compaction for metal retention parameters on COx clay rocks (Chen et al., 2014a; Loni et al., 2021; Montavon et al., 2020); overall, no significant effect was observed. Redox potential is certainly the key parameter; it proves to be even more consistent since uranium is sensitive to redox and the adsorption properties of U(IV) and U(VI) are quite distinct. The potential measured in the solutions prepared in the glove box (and in contact with the clay phases) are oxidizing while that expected under *in-natura* conditions is of the order of -190 mV. This result also aligns with the fact that *in natura* aqueous U concentrations measured in KEY1001 under disturbed oxidizing conditions are higher, i.e. around 2 $\mu g.L^{-1}$, than those representative of the "natural" conditions (0.13-0.25 $\mu g\ L^{-1}$). These concentrations are more closely resembling those predicted by our simple model based on laboratory results (1.4 - 12 $\mu g.L^{-1}$, Fig. 6c).

The following scenario can now be proposed, namely that a more retained form of uranium is present under *in natura* conditions, i.e. the U(IV) form. When the sample is removed from its environment, the U(IV) adsorbed on the surface rapidly oxidizes to U(VI), despite the controlled conditions (with no differences in results between preserved and unpreserved COx samples). In the laboratory, this situation will have the effect of increasing the concentration of aqueous U in suspension since U(VI) is less retained than U(IV). It also explains the

decrease in U concentration in equilibrium with the COx as the solution potential decreases over time; this is the opposite case where the equilibria shift towards the sorption of U(IV) retained to a greater extent by the COx clay fraction than U(VI), even in the presence of the soluble ternary complexes of U(VI) (grey symbols in Fig. 6b).

According to this reasoning, it becomes possible at this stage to return to Rd values more representative of *in natura*/reducing conditions. Using the labile fraction determined from laboratory experiments and the concentration of U found *in natura* (0.25 - 0.13 $\mu g.L^{-1}$), a range of *in natura* Rd between 72 and 323 $L \cdot kg^{-1}$ can be calculated. This Rd value range is in agreement with the value deduced from the desorption experiments performed at -200 mV/NHE and Eq. (2), i.e. 500 ± 200 L kg^{-1}.

This reasoning must now be compared with the predictive calculations derived from the operational model under *in natura* conditions. Results are presented in Figure 6 as a function of P_{CO2} and redox potential, the two key parameters controlling U speciation in the formation. In these calculations, pH is determined such that calcite is considered in equilibrium in a SPW1 type solution. Under conditions expected in the formation (hatched area in the figure), Rd values vary greatly, from 640 to 7,400 $L.kg^{-1}$. From a more mechanistic point of view, the speciation in solution is mainly controlled by U(VI) complexed species, whereas at the surface U(IV) surface complexes govern U speciation (Supplementary data, Fig. S1).

On the one hand, the predicted retention range overestimates the one previously discussed based on experimental data (~70-700 L kg^{-1}). Yet on the other, the same conclusion could still be drawn: ternary U(VI) complexes control U speciation in solution while U(IV) surface species dominate U adsorption. It is also important to recall that predictive approaches give trends, since in addition to working with a complex and heterogeneous natural system (other parameters like clay content affect retention values), uncertainties in the model parameters are

not taken into account. Let's also recall that the parameters for the U(IV)/COx system are extrapolated using the LFER. Therefore, the overlap area between the predicted Rd domain and the Rd domain deduced from experiments allows us to build confidence in our reasoning.

5. CONCLUSION

The aim of this work has been to describe and understand the behavior of U under COx conditions. An operational model based on both a bottom-up approach and the 2SPNE SC/CE model has made it possible to describe the reactivity of U(VI) and U(IV) with respect to COx under laboratory conditions from batch-type experiments. Compared to the accessible databases, it was however necessary to adjust the constant describing the formation ≡S-UO_2-CO_3 ternary surface complexes for illite. Ultimately, it has been well confirmed that the adsorption of uranium onto COx claystone is controlled by the clay phase (and more specifically, illite). Moreover, the COx clay phase is the largest reservoir of naturally-occurring U. In contrast, only a small fraction appears to have been adsorbed (~1 %, namely ~30 $\mu g.kg^{-1}$), i.e. the fraction in rapid exchange equilibrium with the fraction in solution. Depending on the experimental conditions imposed in the laboratory, particularly on the redox potential of the solution, Rd values between ~3 and 700 $L \cdot kg^{-1}$ were obtained in order to characterize the behavior of this labile naturally-occurring U fraction. This variability can mainly be explained by a change in U speciation at the surface, from U(VI) for the lowest Rd values to U(IV) for the highest. Under *in natura* conditions, the results of this work indicate a Rd value > 70 $L.kg^{-1}$, thus reflecting a control of U(IV) at the clay COx surface. This result now needs to be validated by diffusion experiments on intact COx samples.

Acknowledgments

The authors would like to thank the ANDRA Agency (GL CTEC), as well as all contributors to the "*Chaire stockage*" storage study program (EDF, ORANO, ANDRA) for their financial support of this work. This project has also received funding from the European Union's Horizon 2020 research and innovation program under grant agreement No 847593 (EURAD/FUTURE). M. Lundy from ANDRA is to be commended for sending along the information and COx water samples for analysis, as is S. Betelu from the BRGM Institute for measuring the redox potential of the long-term experiment.

Appendices

Table A-1: Characteristics of the COx samples; further details on the characterization method can be found elsewhere (Lerouge et al., 2011)

Sample	Borehole	Depth (m)	Clay fraction (%)	Clay fraction (wt.%)				Carbonate phases	Quartz + Feldspar	Minor phases	
				Illite	$I/S_{(R=0)}$	kaolinite	chlorite			Pyrite	OM
EST51779 / EST51769	OHZ6126	469.72	50	17	28	2	3	25	25	0.8	n.m.
EST05738	EST205	501.50	48.5	20.5	20.5	5	2.5	25	23	0.6	0.8
EST25687	PAC1002	475.92	39.9	3.7	33	1.9	1.3	28	29	1.6	3.9
EST26536	TSF1001	494.32	50	18	31	4.5	3	22	19	0.8	n.m.
EST44346	OHZ1607	489.76	49.5	31.2	16.2	< 1	2.1	24.4	25.5	0.2	1
EST21400	PAC2002	430.10	9.2	2	7.2	< 1	< 1	81	9.1	0.5	0.07
EST26480	FOR1118	490.20	53	21.5	25.5	3	3	24	22	0.8	n.m.
EST05640	EST205	476.57	45	20	23	<1	2	25	27	1.7	n.m.

OM = organic matter; n.m.: not measured

607

608 **Table A-2:** Compositions of the Synthetic Pore Water; concentrations are given in mmol L^{-1}

	pH	Na	K	Mg	Ca	Sr	Cl	SO_4	S(-2)	C(4)	Si	Al	Fe
SPW1	7.2	40.9	1.1	5.3	8.4	0.2	40.2	13.6	_	2.6	n.m.	n.m.	n.m.
SPW2	7	41.7	5.4	9.7	7.7		73.3	4.3	$3.8\ 10^{-10}$	variable	0.094	$9.26\ 10^{-3}$	0.0644

609 n.m.: not measured

610

611 **Table A-3:** Detailed experimental conditions in the U(VI) batch experiments

Sample	Atm-osphere	Solution	m/V (g L^{-1})	Type	Alkalinity (meq/L)	FIG
Illite	Ar(g)	$NaNO_3$ 0.1M	2	Edge; $[U]_0 = 10^{-7}$ M	0.04	1A
Illite	Air	NaCl 0.1M	0.5 – 1	Edge; $[U]_0 = 10^{-7}$ M	0.17	1A
Illite	Ar(g)	$NaNO_3$ 0.1M	2	Isotherm; pH 6.5±0.2	0.07	1B
Illite	Air	$NaNO_3$ 0.1M	2	Isotherm; pH 7.3±0.2	0.23	1B
Illite	1% CO_2	$NaNO_3$ 0.1M	2	Isotherm; pH 7.3±0.1	2.4	1B
Illite	1% CO_2	SPW1	10	Isotherm; pH 7.1±0.2	2.4	1B
Clay fraction	Air	$NaNO_3$ 0.1M	2	Isotherm; pH 7.1	0.22	2A
Clay fraction	1% CO_2	$NaNO_3$ 0.1M	2	Isotherm; pH 7.2	2.4	2A
Clay fraction	1% CO_2	NaCl 0.1M	2	Isotherm; pH 7.3	1.6	2A
Clay fraction	1% CO_2	SPW1	2	Isotherm; pH 7.1	2.5	2A
EST51779	1% CO_2	SPW1	40	Isotherm; pH 7.4	2.5	2B

612

613 **Table A-4:** Detailed experimental conditions in the U(IV) experiments

Sample	Atmosphere	Solution	m/V (g L^{-1})	pH	Eh	$[U]_0$	FIG
EST05640	N_2(g)	SPW2	0.098	8.3	-270 mV	$3{\cdot}10^{-12}$ - 10^{-8} M	3A
EST05640	3,500 ppm CO_2	SPW2	0.098	7.6	-210 mV	$5{\cdot}10^{-12}$ - 10^{-9} M	3B
EST05640	9,500 ppm CO_2	SPW2	0.098	7.1	-203 mV	$4{\cdot}10^{-12}$ - 10^{-9} M	3C

614

615

Table A-5: Surface complexation and cation exchange reactions for the uranium used in modeling. Unless otherwise specified, the constants have been extracted from the Bradbury and Baeyens model (Baeyens and Bradbury, 2017; Bradbury and Baeyens, 2017).

Reactions	Illite (Log K)	Montmorillonite (Log K)
Hexavalent reactions		
$sOH + UO_2^{2+} = sOUO_2^{+} + H^{+}$	2	3.1
$sOH + UO_2^{2+} + H_2O = sOUO_2OH + 2\ H^{+}$	-3.9	-4.6
$sOH + UO_2^{2+} + 2\ H_2O = sOUO_2(OH)_2^{-} + 3H^{+}$	-10.8	-12.6
$sOH + UO_2^{2+} + 3\ H_2O = sOUO_2(OH)_3^{2-} + 4H^{+}$	-18.7	-20.9
$w_1OH + UO_2^{2+} = w_1OUO_2^{+} + H^{+}$	0	0.5
$w_1OH + UO_2^{2+} + H_2O = w_1OUO_2OH + 2\ H^{+}$	-5.8	-5.7
$w_1OH + UO_2^{2+} + 2\ H_2O = w_1OUO_2(OH)_2^{-} + 3\ H^{+}$	(***)	
$sOH + UO_2^{2+} + CO_3^{2-} = sOUO_2CO_3^{-} + H^{+}$	*11.5* (*)	9.8
$sOH + UO_2^{2+} + 2\ CO_3^{2-} = sOUO_2(CO_3)_2^{3-} + H^{+}$	*17.3* (*)	15.5
$w_1OH + UO_2^{2+} + CO_3^{2-} = w_1OUO_2CO_3^{-} + H^{+}$		9.3
$2\ NaX + UO_2^{2+} = UO_2X_2 + 2\ Na^{+}$	0.65	0.146
Tetravalent reactions	(**)	(**)
$sOH + U^{4+} = sOU^{3+} + H^{+}$	7.62	8.24
$sOH + U^{4+} + H_2O = sOUOH^{2+} + 2\ H^{+}$	7.1	7.7
$sOH + U^{4+} + 2\ H_2O = sOU(OH)_2^{+} + 3H^{+}$	3.6	4.0
$sOH + U^{4+} + 3\ H_2O = sOU(OH)_3 + 4H^{+}$	-1.6	-1.4
Amphoteric reactions		
$s/w_1OH + H^{+} = s/w_1OH_2^{+}$	4.0	4.5
$s/w_1OH = s/w_1O^{-} + H^{+}$	-6.2	-7.9
$w_2OH + H^{+} = w_2OH_2^{+}$	8.5	6.0
$w_2OH = w_2O^{-} + H^{+}$	-10.5	-10.5

sOH = strong site (density = 2 µmol/g); w_1OH = weak site (density = 40 µmol/g); w_2OH = weak site (density = 40 µmol/g)

NaX = ion exchange site (CEC illite = 2.25 10^{-4} eq/g, montmorillonite = 8.7 10^{-4} eq/g)

(*) this work

(**) LFER associated with Th^{4+} data: (Montmorillonite: Log $K(S_{x-1})$ = 1.02·Log $K(OH_x)$ + 8.79; illite: Log $K(S_{x-1})$ = 0.97·Log $K(OH_x)$ + 8.14)

(***) Note that the equilibrium leading to the surface species $w_1UO_2(OH)_2$ was not considered because its contribution in our experimental conditions could be neglected

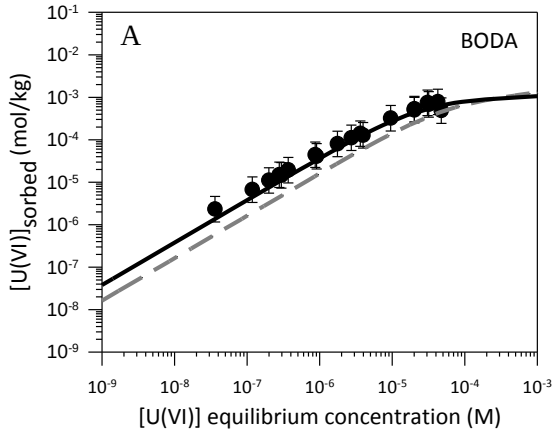

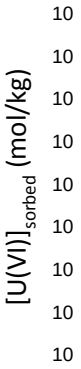

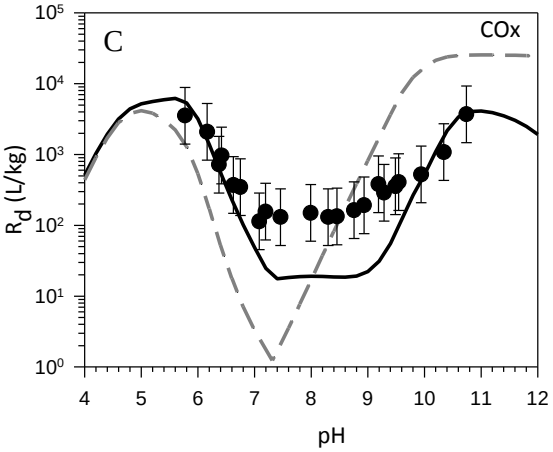

630 **Figure A-1:** Adsorption of uranium on clay minerals in equilibrium atmospheric CO_2.
631 (A) BODA Claystone (Marques Fernandes et al., 2015); (B) OPA Claystone (Marques
632 Fernandes et al., 2015) (MF15) and (Joseph et al., 2011) (JOS11); (C) COx claystone in 0.1 M
633 $NaClO_4$ (Hartmann et al., 2008). Symbols = experimental data. The grey dashed lines
634 represent the published model. The black lines correspond to our adjusted model (Table A5).
635

636

REFERENCES

Ahmed, H.M.M. (2014) Lability and solubility of uranium and thorium in soil. University of Nottingham, p. 290.

Altmann, S. (2008) 'Geo'chemical research: A key building block for nuclear waste disposal safety cases. Journal of Contaminant Hydrology 102, 174-179.

Amayri, S., Fröhlich, D.R., Kaplan, U., Trautmann, N. and Reich, T. (2016) Distribution coefficients for the sorption of Th, U, Np, Pu and Am on Opalinus Clay. Radiochimica Acta 104, 33-40.

ANDRA (2005) Dossier 2005. Andra research on the geological disposal of high-level long-lived radioactive waste. Results and perspectives. ANDRA, Châtenay-Malabry (France).

Baeyens, B. and Bradbury, M. (2017) The development of a thermodynamic sorption data base for montmorillonite and the application to bentonite, PSI Bericht 17-05.

Bernhard, G., Geipel, G., Brendler, V. and Nitsche, H. (1996) Speciation of Uranium in seepage waters of a mine tailing pile studied by Time-Resolved Laser-Induced Fluorescence Spectroscopy (TRLFS). Radiochimica Acta 74, 87-91.

Bradbury, M. and Baeyens, B. (2017) The development of a thermodynamic sorption data base for illite and the application to argillaceous rocks, PSI Bericht 17-06.

Bradbury, M.H. and Baeyens, B. (1997) A mechanistic description of Ni and Zn sorption on Na-montmorillonite Part II: modelling. Journal of Contaminant Hydrology 27, 223-248.

Bradbury, M.H. and Baeyens, B. (2011) Predictive sorption modelling of Ni(II), Co(II), Eu(III), Th(IV) and U(VI) on MX-80 bentonite and Opalinus Clay: A "bottom-up" approach. Applied Clay Science 52, 27-33.

Chen, Z., Montavon, G., Guo, Z., Wang, X., Razafindratsima, S., Robinet, J.C. and Landesman, C. (2014a) Approaches to surface complexation modeling of Ni(II) on Callovo-Oxfordian clayrock. Applied Clay Science 101, 369-380.

Chen, Z., Montavon, G., Ribet, S., Z., G., Robinet, J.C., David, K., Tournassat, C., Grambow, B. and Landesman, C. (2014b) Key factors to understand in-situ behavior of Cs in Callovo–Oxfordian clay-rock (France). Chemical Geology 387, 47-58.

Claret, F., Lerouge, C., Laurioux, T., Bizi, M., Conte, T., Ghestem, J.P., Wille, G., Sato, T., Gaucher, E.C., Giffaut, E. and Tournassat, C. (2010) Natural iodine in a clay formation: Implications for iodine fate in geological disposals. Geochimica et Cosmochimica Acta 74, 16-29.

Claret, F., Sakharov, B.A., Drits, V.A., Velde, B., Meunier, A., Griffault, L. and Lanson, B. (2004) Clay minerals in the Meuse-Haute Marne underground laboratory (France): possible influence of organic matter on clay mineral evolution. Clay Clay. Miner. 52, 515–532.

Curtis, G.P., Fox, P., Kohler, M. and Davis, J.A. (2004) Comparison of in situ uranium K_D values with a laboratory determined surface complexation model. Applied Geochemistry 19, 1643-1653.

Davies, C.W. (1962) Ion association, in: Buttterworths (Ed.), London.

673 Dong, W. and Brooks, S.C. (2006) Determination of the formation constants of ternary complexes of
674 uranyl and carbonate with alkaline earth metals (Mg^{2+}, Ca^{2+}, Sr^{2+}, and Ba^{2+}) using anion exchange
675 method. Environmental Science and Technology 40, 4689-4695.

676 Fralova, L. (2020) Transport diffusif de l'uranium dans la roche argileuse du Callovo-Oxfordien,
677 mécanismes et sensibilité aux perturbations chimiques. Université Paris sciences et lettres.

678 Gaucher, E.C., Tournassat, C., Pearson, F.J., Blanc, P., Crouzet, C., Lerouge, C. and Altmann, S. (2009)
679 A robust model for pore-water chemistry of clayrock. Geochimica et Cosmochimica Acta 73, 6470-
680 6487.

681 Grangeon, S., Vinsot, A., Tournassat, C., Lerouge, C., Giffaut, E., Heck, S., Groschopf, N., Denecke,
682 M.A., Wechner, S. and Schäfer, T. (2015) The influence of natural trace element distribution on the
683 mobility of radionuclides. The exemple of nickel in a clay-rock. Applied Geochemistry 52, 155-173.

684 Grenthe, I., Gaona, X., Plyasunov, A., Rao, L., Runde, W.H., Grambow, B., Konings, R.J.M., Smith, A.L.
685 and Moore, E.E. (2020) Second update on the chemical thermodynamics of Uranium, Neptunium,
686 Plutonium, Americium and Technetium. OECD Nuclear Energy Agency, Data Bank, Boulogne-
687 Billancourt (France).

688 Grivé, M., Duro, L., Colas, E. and Giffaut, E. (2015) Thermodynamic data selection applied to
689 radionuclides and chemotoxic elements: An overview of the ThermoChimie-TDB. Applied
690 Geochemistry 55, 85-94.

691 Guillaumont, R., Fanghanel, T., Neck, V., Fuger, J., Palmer, D.A., Grenthe, I. and Rand, M.H. (2003)
692 Update on the chemical thermodynamics of Uranium, Neptunium, Plutonium, Americium and
693 Technetium. OECD Nuclear Energy Agency, Data Bank, Issy-les-Moulineaux (France).

694 Hartmann, E., Geckeis, H., Rabung, T., Lutzenkirchen, J. and Fanghanel, T. (2008) Sorption of
695 radionuclides onto natural clay rocks. Radiochimica Acta 96, 699-707.

696 Hennig, T., Stockmann, M. and Kühn, M. (2020) Simulation of diffusive uranium transport and
697 sorption processes in the Opalinus Clay. Applied Geochemistry 123, 104777.

698 Joseph, C., Schmeide, K., Sachs, S., Brendler, V., Geipel, G. and Bernhard, G. (2011) Sorption of
699 uranium(VI) onto Opalinus Clay in the absence and presence of humic acid in Opalinus Clay pore
700 water. Chemical Geology 284, 240-250.

701 Kautenburger, R., Brix, K. and Hein, C. (2019) Insights into the retention behaviour of europium(III)
702 and uranium(VI) onto Opalinus Clay influenced by pore water composition, temperature, pH and
703 organic compounds. Applied Geochemistry 109, 104404.

704 Kohler, M., Curtis, G.P., Meece, D.E. and Davis, J.A. (2004) Methods for estimating adsorbed
705 uranium(VI) and distribution coefficients of contaminated sediments. Environmental Science and
706 Technology 38, 240-247.

707 Lerouge, C., Grangeon, S., Gaucher, E.C., Tournassat, C., Agrinier, P., Guerrot, C., Widory, D., Fléhoc,
708 C., Wille, G., Ramboz, C., Vinsot, A. and Buschaert, S. (2011) Mineralogical and isotopic record of
709 biotic and abiotic diagenesis of the Callovian-Oxfordian clayey formation of Bure (France).
710 Geochimica et Cosmochimica Acta 75, 2633-2663.

Lerouge, C., Michel, P., Gaucher, E.C. and Tournassat, C. (2006) A geological, mineralogical and geochemical GIS for the Andra URL: a tool for the water–rock interactions modelling at a regional scale, 2nd annual workshop - FUNMIG, Stockhom Sweden.

Loni, Y.H., David, K., Ribet, S., Lach, P., Lerouge, C., Made, B., Bailly, C., Grambow, B. and Montavon, G. (2021) Investigation of europium retention on Callovo-Oxfordian clay rock (France) by laser ablation inductively coupled plasma mass spectrometry (LA-ICP-MS) and percolation experiments in microcells. Applied Clay Science 214.

Maia, F.M.S., Ribet, S., Bailly, C., Grivé, M., Madé, B. and Montavon, G. (2021) Evaluation of thermodynamic data for aqueous Ca-U(VI)-CO_3 species under conditions characteristic of geological clay formation. Applied Geochemistry 124, 104844.

Marques Fernandes, M., Baeyens, B., Dähn, R., Scheinost, A.C. and Bradbury, M.H. (2012) U(VI) sorption on montmorillonite in the absence and presence of carbonate: A macroscopic and microscopic study. Geochimica et Cosmochimica Acta 93, 262-277.

Marques Fernandes, M., Vér, N. and Baeyens, B. (2015) Predicting the uptake of Cs, Co, Ni, Eu, Th and U on argillaceous rocks using sorption models for illite. Applied Geochemistry 59, 189-199.

McKinley, I.G. and Alexander, W.R. (1993) Assessment of radionuclide retardation: uses and abuses of natural analogue studies. Journal of Contaminant Hydrology 13, 249-259.

Montavon, G., Alhajji, E. and Grambow, B. (2006) Study of the interaction of Ni^{2+} and Cs^{+} on MX-80 bentonite; Effect of compaction using the "capillary method". Environmental Science and Technology 40, 4672-4679.

Montavon, G., Lerouge, C., David, K., Ribet, S., Hassan-Loni, Y., Leferrec, M., Bailly, C., Robinet, J.-C. and Grambow, B. (2020) Nickel retention on Callovo-Oxfordian clay: Applicability of existing adsorption models for dilute systems to real compact rock. Environmental Science and Technology 54, 12226-12234.

OECD Nuclear Energy Agency (2002) Radionuclide retention in geologic media, NEA Report. OECD, p. 269.

Parkhurst, D.L. and Appelo, C.A.J. (2013) Description of input and examples for PhreeqC Version 3 – A computer program for speciation, batch-reaction, One-dimensional transport and inverse geochemical calculations. Water-resources investigations Report, Denver, CO USA, p. 519.

Payne, T.E., Edis, R., Fenton, B.R. and Waite, T.D. (2001) Comparison of laboratory uranium sorption data with ‘in situ distribution coefficients’ at the Koongarra uranium deposit, Northern Australia. Journal of Environmental Radioactivity 57, 35-55.

Regenspurg, S., Margot-Roquier, C., Harfouche, M., Froidevaux, P., Steinmann, P., Junier, P. and Bernier-Latmani, R. (2010) Speciation of naturally-accumulated uranium in an organic-rich soil of an alpine region (Switzerland). Geochimica et Cosmochimica Acta 74, 2082–2098.

Rieder, F. (2019) Impact of competing anions on the sorption of trivalent actinides onto clay mineral surfaces. KIT-Fakultät für Chemie und Biowissenschaften.

Tournassat, C., Gailhanou, H., Crouzet, C., Braibant, G., Gautier, A. and Gaucher, E.C. (2009) Cation Exchange Selectivity Coefficient Values on Smectite and Mixed-Layer Illite/Smectite Minerals. Soil Science Society of America Journal 73, 928-942.

751 Tournassat, C., Tinnacher, R.M., Grangeon, S. and Davis, J.A. (2018) Modeling uranium(VI) adsorption
752 onto montmorillonite under varying carbonate concentrations: A surface complexation model
753 accounting for the spillover effect on surface potential. Geochimica et Cosmochimica Acta 220, 291-
754 308.

755 Vinsot, A., Linard, Y., Lundy, M., Necib, S. and Wechner, S. (2013) Insights on desaturation processes
756 based on the chemistry of seepage water from boreholes in the Callovo-Oxfordian argillaceous rock
757 Procedia Earth and Planetary Science 7, 871 – 874

758 Zhao, M.-Y. and Zheng, Y.-F. (2014) Marine carbonate records of terrigenous input into Paleotethyan
759 seawater: Geochemical constraints from Carboniferous limestones. Geochimica et Cosmochimica
760 Acta 141, 508-531.
761

762

763

764

765

766 **Table 1:** Summary of the experiments conducted in this study

Objective	Samples		Tasks	Conditions	Corresponding Figure(s) and/or Table
Model building	Illite	Purified	Evaluation of the carbonate effect on U adsorption onto illite	SPW1 / 0.1M NaCl / 0.1M $NaNO_3$ Ar / $P_{CO2} = 10^{-3.5} / 10^{-2} / 10^{-1.3}$ pH: 4 - 9.8 m/V: 2 g/L $[U]_0 = 10^{-9} - 2{\cdot}10^{-5}$ M	Figure 1 Table A
	COx-clay fraction	Purified from EST51779	Model testing on the COx clay fraction	0.1M $NaNO_3$ / SPW1 $P_{CO2} = 10^{-3.5} / 10^{-2}$ pH: 6.7 - 7.1 m/V: 2 g/L $[U]_0 = 5{\cdot}10^{-8} - 2{\cdot}10^{-5}$ M	Figure 2A Table A
	COx claystone	EST51779	Model testing on the COx under oxidizing conditions	SPW1 $P_{CO2} = 10^{-2}$ pH: 7.4 m/V: 40 g/L $[U]_0 = 5{\cdot}10^{-8} - 2{\cdot}10^{-5}$ M	Figure 2B Table A
	COx claystone	EST05640	Model testing on the COx under reducing conditions	SPW2 $N_2 / P_{CO2} = 10^{-3.5} / 10^{-2}$ Eh -185 mV pH: 7.1 - 8.3 m/V: 0.1 g/L $[U]_0 = 3{\cdot}10^{-12} - 10^{-8}$ M	Figure 3 Table B
Naturally-occurring Uranium	COx claystone	EST51769 / EST05738 / EST26536	Uranium distribution and solid analyses	—	Table S1 Figure 4C
		EST25687 / EST25687(ox) / EST21400 / EST26536 / EST26480	Sequential extraction	See Section 2.2	Figure 4
		EST44346	Determination of the labile fraction	SPW1 $[^{233}U] = 3.10^{-10}$ M Isotope exchange method	Figure 5
		EST25687(ox) / EST51779		SPW1 Desorption method	

767

768

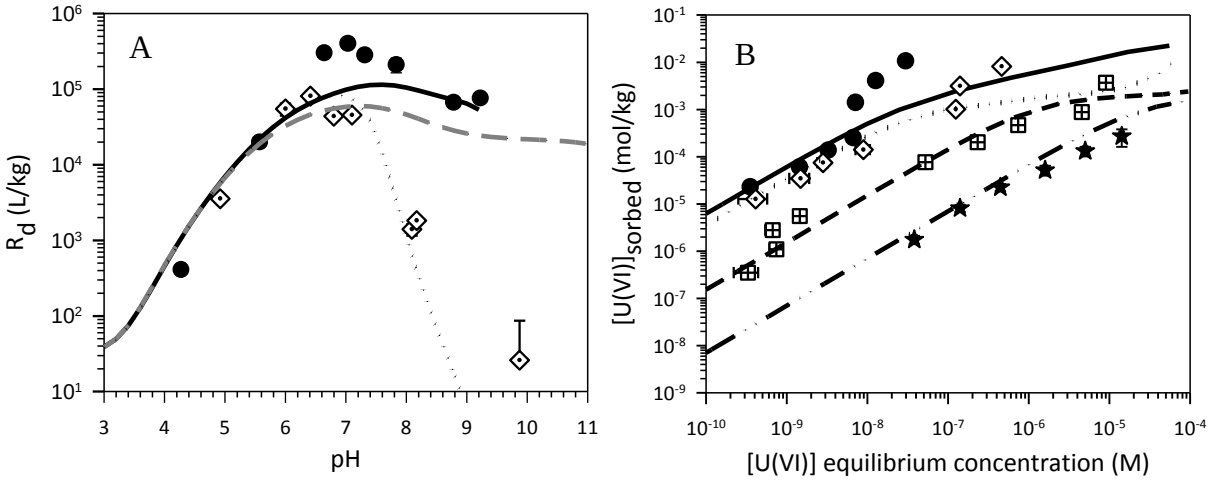

Figure 1: Adsorption of U(VI) onto illite under various experimental conditions (see Tables 1 and A3). (A) variation vs. pH, (B) concentration isotherms. Symbols = experimental data (circle: 0.1 M $NaNO_3$ in ~Ar atmosphere, diamond: 0.1 M $NaNO_3$ in ~atmospheric CO_2; square: 0.1 M $NaNO_3$ or NaCl in ~1% CO_2, star = SPW1 in ~1% CO_2). The grey dashed line depicts the model for 0.1 M $NaClO_4$ and CO_2 free atmosphere without considering the surface complexes with carbonates. Black lines correspond to our adjusted model (Table A5).

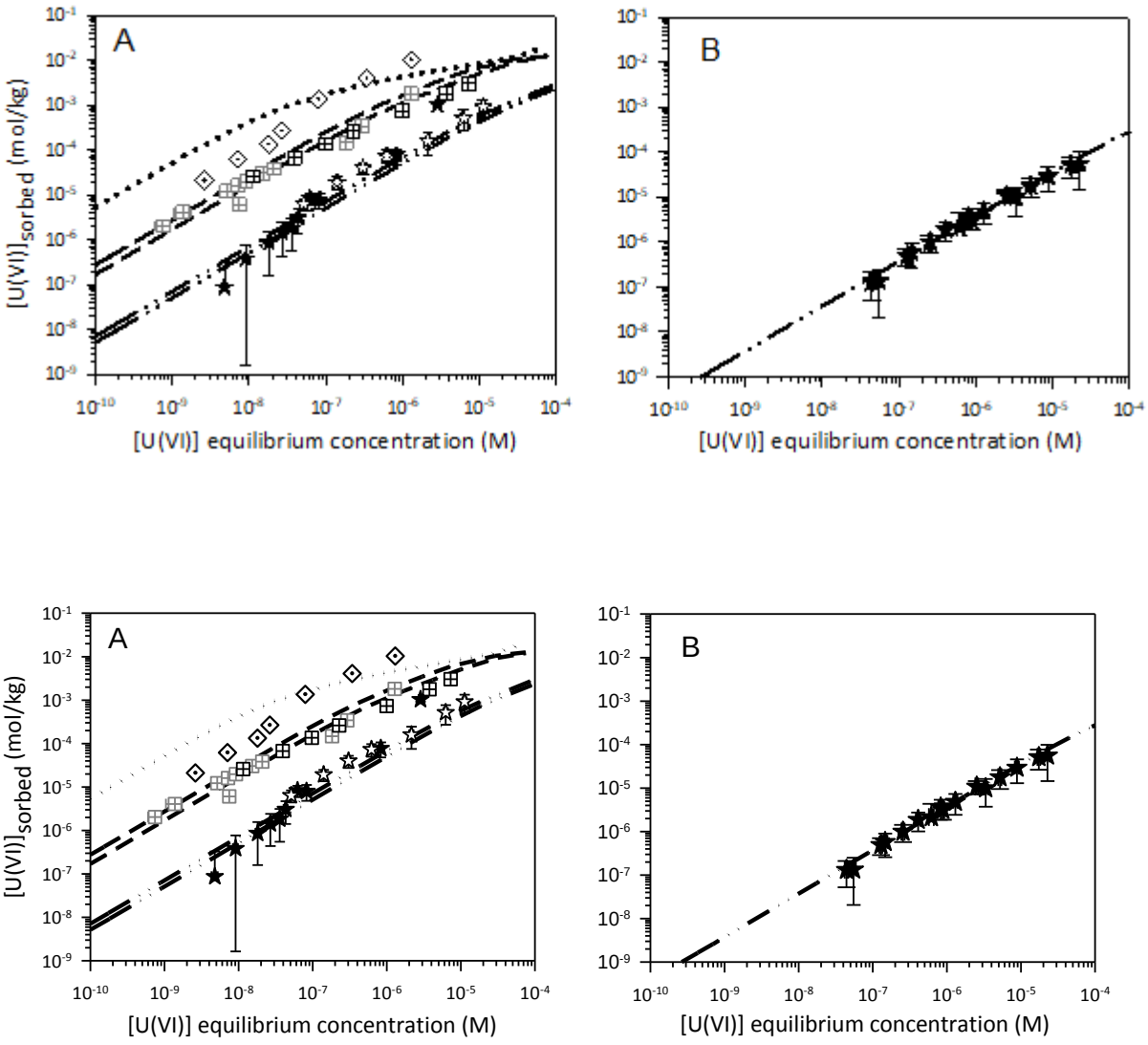

Figure 2: Adsorption of uranium(VI) on: (A) COx clay fraction, and (B) COx rock (see Tables 1 and A3). Symbols = experimental data (diamond: ~atmospheric CO_2 pressure, square: 0.1 M $NaNO_3$ or NaCl in ~1% CO_2, star = SPW1 composition in 1% CO_2). The lines correspond to our adjusted model (Table A5).

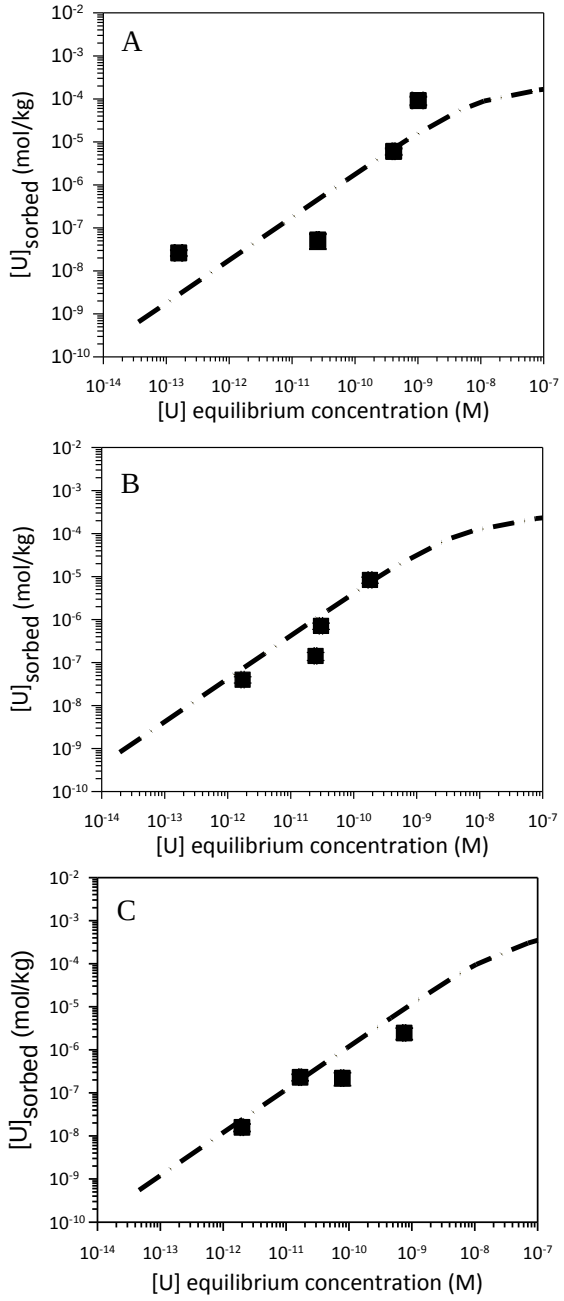

Figure 3: Adsorption of uranium on COx under reducing conditions for various atmospheres: (A) Ar (pH = 8.3, Eh = -265 mV), (B) air (pH = 7.5, Eh = -215 mV), and (C) 1% CO2 (pH = 7.1, Eh = -201 mV) (see Table B). The lines depict the model results (modeling parameters are given in Table A5).

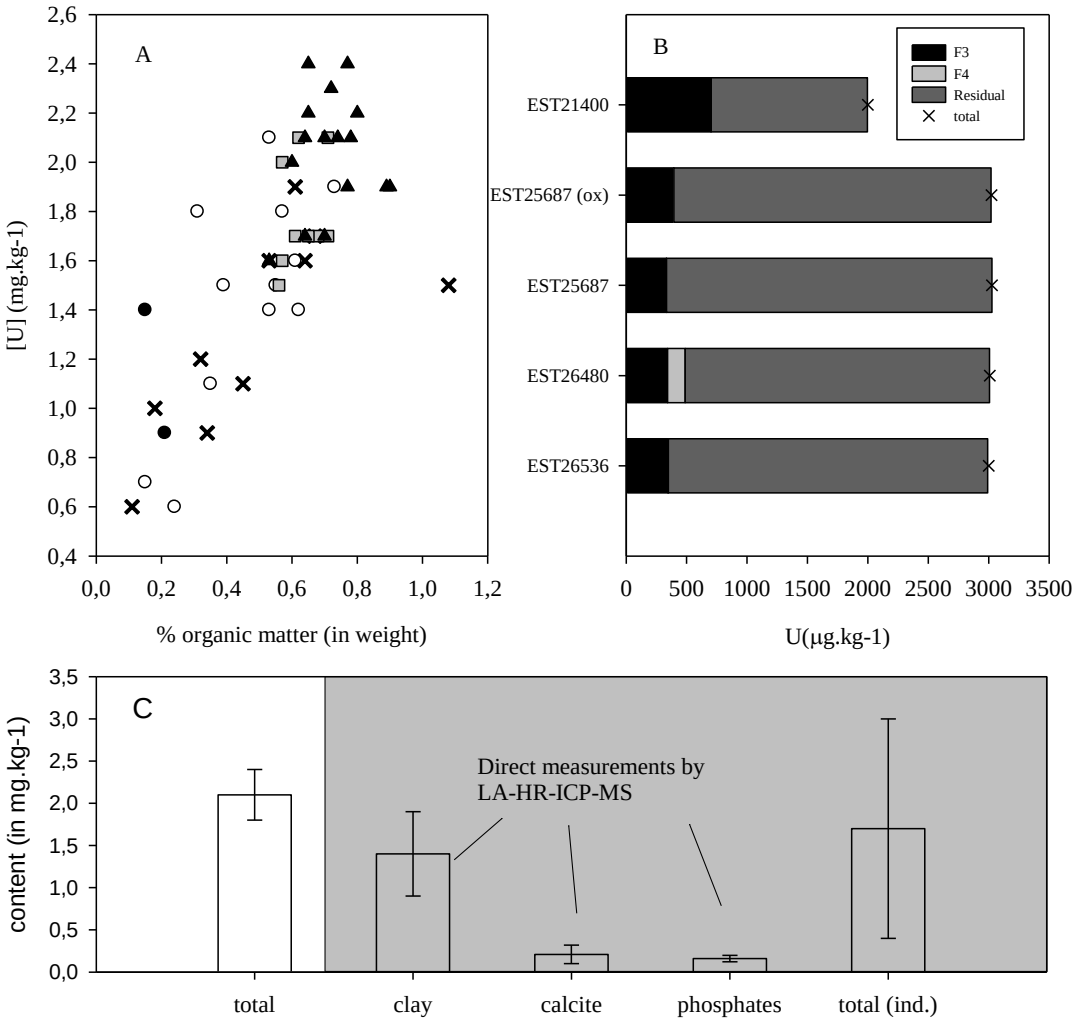

Figure 4: Naturally-occurring U in the COx: (A) U content vs. organic matter content. (B) Sequential extraction results; the U concentrations in Fractions 1 and 2 are not shown here due to their weak contribution. (C) Distribution of U between the various selected phases; all values are given in Table S3.

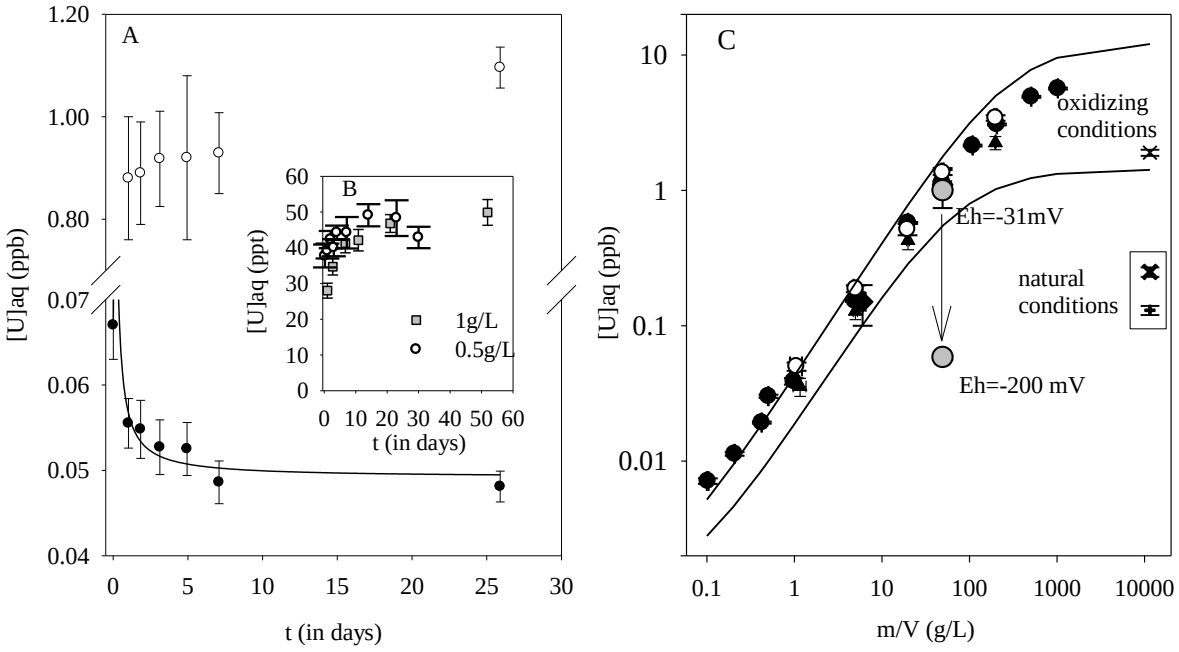

Figure 5: Results of equilibrium-based methods. (A) Isotopic exchange method with S/L = 49.5 g/L; U-238 (O) and U-233 (●) concentrations measured over time. The line shows a trend curve. (B) U-238 concentration measured over time. (C) Desorption method; the dark symbols correspond to three data series (EST51779, etc.); the white symbol represents the series with EST25687(ox); and the gray symbol denotes the experiment performed over a long contact time. The lines depict the fitting/calculation results (Eq. 2) (see text). The symbols on the right reflect concentrations measured directly in the pore water under preserved and unpreserved conditions.

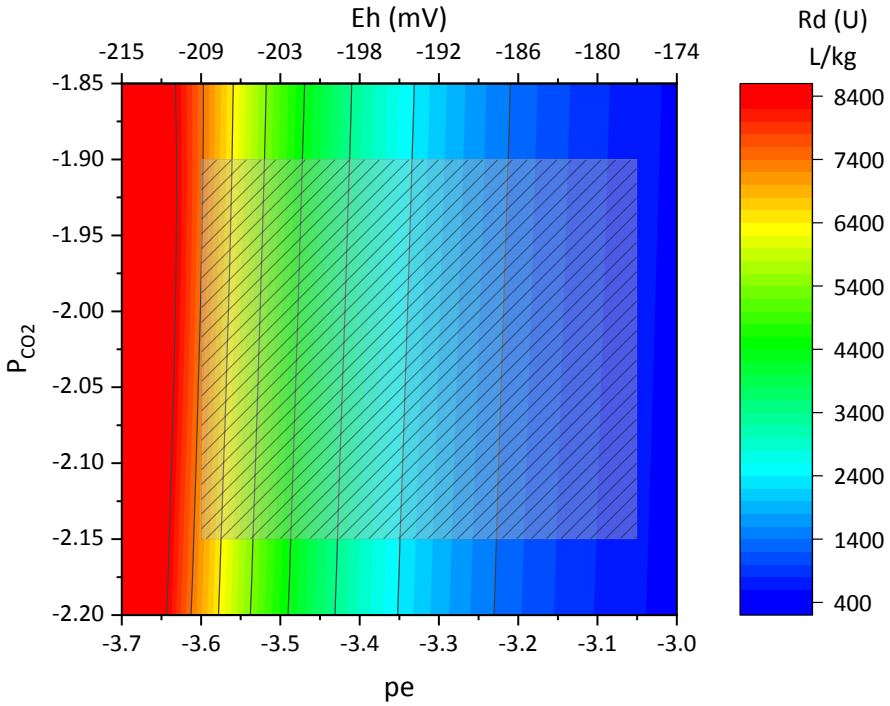

Figure 6: Variation in the distribution coefficient under *in natura* conditions vs. pe and P_{CO2} (pH determined for calcite equilibrium, with [Ca]=8.4 mmol/L). The hatched area corresponds to expected *in natura* conditions.